Sensors & Transducers, Vol. 27, Special Issue, May 2014, pp. 174-179

www.sensorsportal.com

Sensors & Transducers

http://www.sensorsportal.com

V and Nb Influence on the Austenitic Stainless Steel Corrosion in 0.1 M HCl

Amel GHARBI, Kamel MADDOURI, Abdelaziz HIMOUR, Sihem ABDERRAHMANE and Sameh ATHMANI

Surface Engineering Laboratory (L.I.S), Badji Mokhtar University,
B.P.12-23000, Annaba, Algeria
Tel.: +213 (0) 670 05 67 20, fax: +213- 38 86 14 16
E-mail: ahimour@yahoo.fr

Received: 31 December 2012 /Accepted: 10 August 2013 /Published: 26 May 2014

Abstract: Vanadium and niobium were added in AISI309 austenitic stainless steel composition to modify their structure and pitting corrosion resistance in 0.1 M HCl. The structural characterization was carried out by X-rays diffraction and optical microscopy. Corrosion behavior was investigated using potentiodynamic tests and electrochemical impedance measurements (EIS) .Results showed that vanadium and niobium addition precipitated stable carbides (VC, NbC) to chromium carbides' detriment and improved austenitic stainless steel corrosion resistance. *Copyright © 2014 IFSA Publishing, S. L.*

Keywords: Stainless steel, Intergranular precipitation, Corrosion, Vanadium, Niobium, EIS.

1. Introduction

Austenitic stainless steels (ASS) are well known metallic materials; they are widely used in industry: food and beverage, chemical, nuclear, transport and even, recently, in structural uses [1-8]. They have relatively low cost and excellent resistance to uniform corrosion [9, 10]. However, they are prone to localized corrosion such as crevice, pitting, intergranular and intergranular stress corrosion. The intergranular sensitivety is due to carbides rich in chromium formed along the grain boundaries. This process provokes chromium impoverishment in the immediate vicinity. When chromium percentage is below 12 % the depleted areas become prone to corrosion [11–13].

To protect ASS from corrosion, structural stabilization is necessary. The stabilizing elements' addition to ASS produces several beneficial effects such as intergranular corrosion reduction, void swelling and precipitate strengthening [14]. MC (M = V, Nb, Ti, Zr, Ta) carbides are very stable and invariably present in ASS. Their aim is to reduce $M_{23}C_6$ (M = Cr, Fe, Mo) carbides' precipitation and its undesirable consequences, particularly susceptibility to corrosion [14, 15].

Niobium addition in ASS enhances the mechanical properties at high temperatures [16] and increases the localized corrosion resistance in NaCl [2]. Vanadium addition (0.5 - l.0 %) wt. increases the ASS resistance properties without any effect on ductility [17]. Vanadium and Niobium combined addition in ASS is called double stabilization; it has the following advantages: high resistance to raised temperature and better aqueous corrosion resistance. In this work, we study V and Nb effect on the AISI309 austenitic stainless steel corrosion in 0.1 M HCl.

Article number P_SI_497

2. Experimental

2.1. Materials

Alloys chemical composition is cited in Table 1. Samples solution treatment is carried out at a temperature of 1100 °C for 4 h then quenched in water.

For metallographic examination, samples are gradually polished by various abrasive papers: 80, 180, 400, 600, 800, and 1200, followed by paste diamond (3µm) polishing. Then, they are chemically attacked by Catella reagent: 10 cm^3 HCl, 6 cm^3 CH_3COOH, 2g picric acid, 100 cm^3 $C_2H_5O_{14}$ [18].

Table 1. ASS Chemical composition (wt %).

Steel	C	Si	Mn	P	S	Al	Cr	Ni	Nb	V
AISI309 (A)	0.4	1.58	0.74	0.01	0.01	0.3	23.9	14.2	-	0.08
AISI309+ 0.14%Nb +1.2%V (B)	0.4	1.54	0.79	0.01	0.01	0.2	23.9	14	0.14	1.2

The X-rays diffraction is used for the quantitative and qualitative microstructural analysis of the existing phases, mainly austenitic and carbides. X-rays diffraction spectra are obtained using X-rays "PHILIPS" diffractometer, equipped with copper anticathode tube ($\lambda_{K\alpha}$=1,54Å), the spectrum is fitted through the Rietveld method.

2.2. Electrochemical Measurements

Electrochemical measurements are carried out with potentiostat/galvanostat PGZ 301 (Radiometer Analytical-France); associated with Volta-Master 4 software and a classical three electrodes Pyrex cell: Platinum counter electrode, saturated calomel reference electrode (ECS) and working steel electrode which is coated in epoxy resin, except 1 cm^2 section. Before each test, the section surface is polished with grain size abrasive paper from 600 to 2400, then with diamond paste (3 µm). After that, it is degreased with acetone, rinsed with distilled water and at last dried under airflow.

Potentiodynamic curves are plotted in potentials' range (-600 - +600) mV/ECS at 1 mV/s scan rate in 0.1 M HCl aerated solution.

Electrochemical impedance spectroscopy (EIS) measurements were carried out in the frequency range of 100 kHz to 10 MHz, at the open circuit potential using 10 mV amplitude. Transfer resistance R_{ct} and electrical double layer capacitance C_{dl} are determined by Nyquist analysis and the equivalent circuit is determined with Z-view software.

3. Results and Discussion

3.1. Microstructure

Fig. 1 shows steels A and B microstructures; they are composed of austenitic matrix in beige color and precipitates in green color. These latters are in both grain boundaries and grain interiors; steel B boundaries grains' precipitates quantity is lower than in steel A. Nevertheless, this technique does not allow each phase identification.

The X-rays diffraction method is also used to characterize microstructures; the results are shown in Fig. 2. For steel A (Fig. 2a), the phases are mainly: gamma-Fe (Fe_γ), carbides Cr_7C_3, $Cr_{23}C_6$ and oxides: Cr_2O_3, CrO_3; whereas, for steel B (Fig. 2b) the identified phase are predominant: gamma-Fe (Fe_γ), carbides $M_{23}C_6$, Cr_7C_3, VC, NbC and oxides Cr_2O_3, CrO_3. Table 2 presents the each phase proportion; these results are deduced from diffraction spectra by using Reitveld method and software MAUD.

These results' analysis show that vanadium and niobium addition in steel A reduces the intergranular precipitation quantity of primary Cr_7C_3 and secondary $Cr_{23}C_6$ carbides from 17 % to 16 % and 15 % to 10 % respectively.

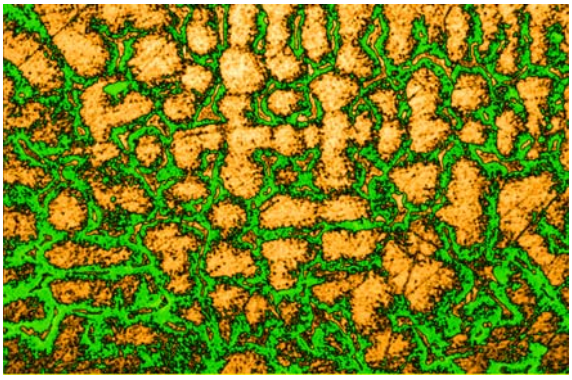

(a)

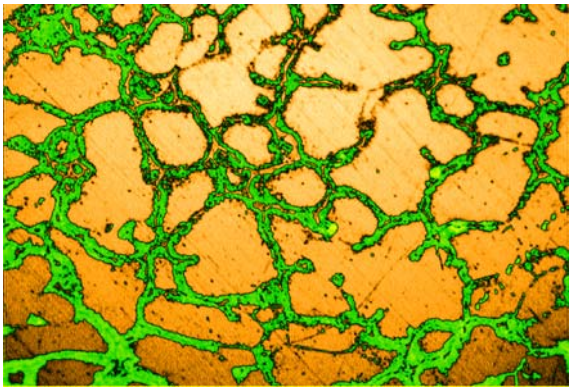

(b)

Fig. 1. Metallographic structures (X400): (a) steel A; (b) steel B.

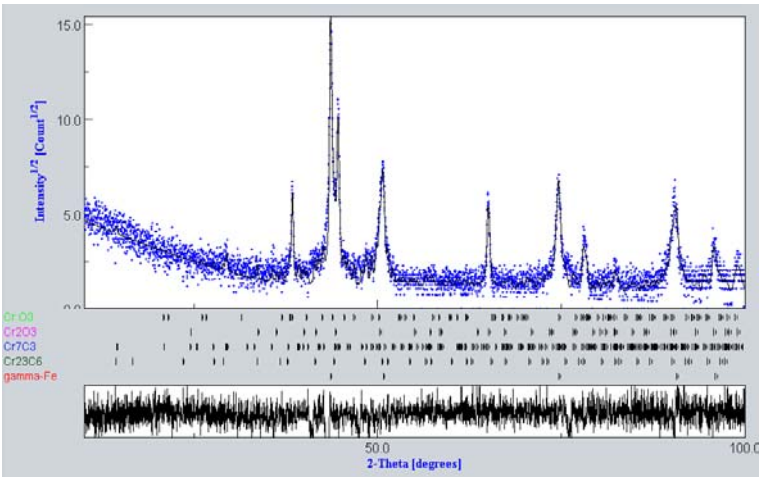

(a)

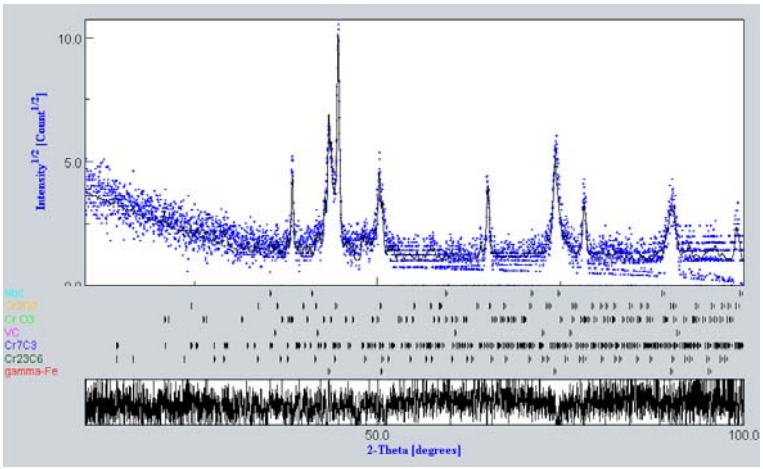

(b)

Fig. 2. X-ray diffractograms: (a) steel A; (b) steel B.

Table 2. Phases proportion (%) in both steels.

Steel	Fe_γ	$Cr_{23}C_6$	Cr_7C_3	NbC	VC	CrO_3	Cr_2O_3
A	54.9	15.55	17.55	-	-	4.19	7.73
B	66.4	10.11	16.68	0.027	2.053	2.31	5.23

3.1. Potentiodynamic Polarization Measurements

Fig. 3 shows potentiodynamic polarization curves for steel A and steel B in 0.1M HCl. Both steels curves shape is substantially identical; we note passive domain absence. It is attributed to synergetic interaction that exists between the Cl^- ions chemisorbed on metallic surface and H^+ ions from the solution. These latters are electrostatically attracted by Cl^- ions that cover the metallic surface and catalyze the dissolution reactions [19-22].

The obtained electrochemical parameters (E_{corr}; I_{corr}) are (-449 mV; 0.038 mA.cm^{-2}) and (-385 mV; 0.012 mA.cm^{-2}) for steel A and steel B respectively (Table 3).

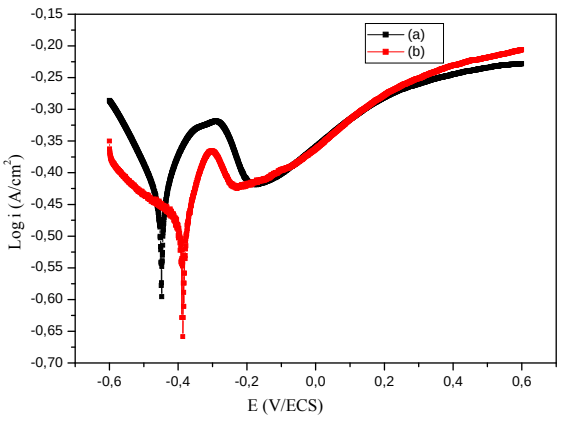

Fig. 3. Potentiodynamic curves obtained in 0.1 M HCl: (a) steel A, (b) steel B.

Vanadium and Niobium addition in steel A displaces the corrosion potential towards nobler

values and decreases the corrosion current density. Anodic and cathodic Tafel constants are (β_a=70.4; β_c=91.3) mVdecade^{-1}and (β_a=49.8; β_c=204) mV decade^{-1}for steel A and steel B respectively. These results show that Vanadium and Niobium addition reduces partially anodic current.

Table 3. Electrochemical parameters deduced from Potentiodynamic curves.

Steel	E_{corr} (mV)	I_{corr} (mA/ cm^2)	β_a (mV dec^{-1})	β_c (mV dec^{-1})	Rp (Ω.cm^2)
A	-449	0.038	70.4	91.3	390
B	-385	0.012	49.8	204	1340

3.2. Electrochemical Impedance Measurements

Fig. 4 shows the Nyquist diagrams for steel A and steel B in 0.1 M HCl. Impedance diagrams are composed of capacitive loop at high-frequency and inductive loop at low-frequency.

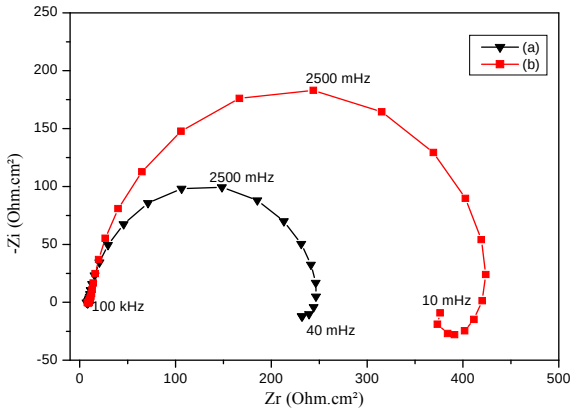

Fig. 4. Nyquist plots: (a) steel A, (b) steel B in 0.1 M HCl.

The capacitive loop can be attributed to the charge transfer reaction and time constant of the electric double layer. The capacitive loop radius variation is linked to stainless steel (AISI309) passivation process in an aerated solution [23, 24]. Inductive loop at low frequencies can represent the incubation period beginning for pitting corrosion [13]. Bode plots Fig. 5 refers to equivalent circuit existence that contains a single constant phase element in metal/solution interface.

EIS data are analyzed using the software Zview, we obtain for both steel A and steel B the same equivalent circuit model shown in Fig. 6. Whereas, various parameters have different values as cited in Table 4. This circuit consists of resistance solution (R_s), the double layer capacitance (C_{dl}) and charge transfer resistance (R_{ct}), R_L and L are the resistance and inductance respectively.

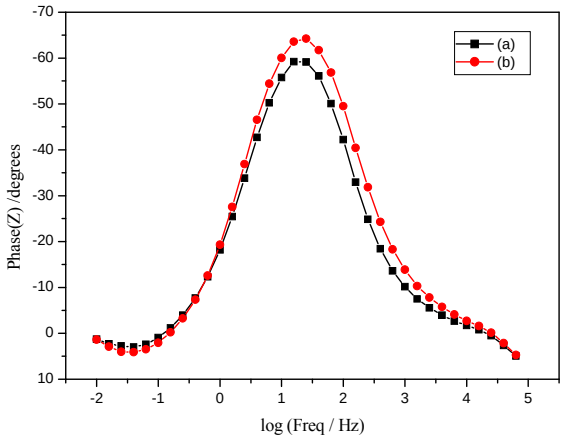

(a)

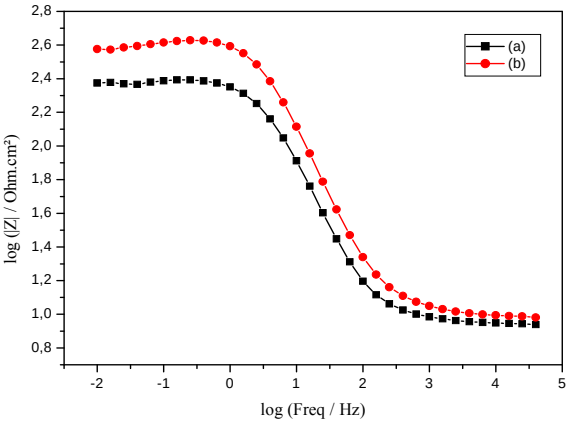

(b)

Fig. 5. Bode diagrams: (a) steel A, (b) steel B in 0.1M HCl.

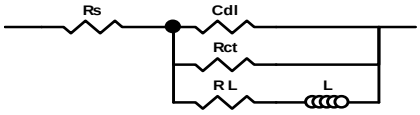

Fig. 6. Equivalent circuit representing impedance spectra of steels A and B.

Table 4. Fitting results of impedance spectra of steels A and B.

Steel	Re Ω cm^{-2}	C_{dl} μF.cm^{-2}	n	R_{ct} Ω cm^{-2}	R_L Ω cm^{-2}	L H
A	9	316.1	0.873	246	1479	4570
B	10	189.5	0.883	437	2074	5151

These results' analysis shows that vanadium and niobium addition in austenitic stainless steel AISI309 increases the charge transfer resistance R_{ct} and reduces the double layer capacitance C_{dl}.

A large R_{ct} is associated with a slower corroding system. Furthermore, a better protection is associated with a decrease in C_{dl}, which results from a decrease in local dielectric constant and/or an increase in the thickness of the electrical double layer [24].

4. Conclusions

Vanadium and niobium are added in AISI309 austenitic stainless steel composition to modify their structure and pitting corrosion resistance in 0.1 M HCl.

Microstructures characterization shows that the addition elements (steel B) reduce the intergranular carbides precipitations' quantity: primary Cr_7C_3 from 17 % to 16 % and secondary $Cr_{23}C_6$ from 15 % to10 %.

Electrochemical parameters values (E_{corr}; I_{corr}) are (-449 mV; 0.038 mA.cm^{-2}) and (-385; 0.012 mA.cm^2) for steel A and steel B respectively. Vanadium and Niobium addition displace the corrosion potential towards nobler values and decreases the corrosion current density.

Impedance measurements confirm these results for steel A and steel B respectively: charge transfer resistance (R_{ct}) increases from 246 to 437 Ω cm^{-2} and double layer capacitance C_{dl} decreases from 316.1 to 189.5 μF.cm^{-2}.

Vanadium and niobium addition in AISI309 austenitic stainless steel provokes vanadium and niobium stable carbides precipitation at the expense of chromium carbides. This microstructure has a better resistance to pitting corrosion in 0.1 M HCl.

Acknowledgements

The authors thank Mrs. Nora ZENNADI for helping them to translate this work.

References

[1]. M. K. Lei, X. M. Zhu, In vitro corrosion resistance of plasma source ion nitride austenitic stainless steels, *Biomaterials*, Vol. 22, 2001, pp. 641-647.

[2]. Abdel Salam Hamdy, Eman El-Shenawy, T. El-Bitar, The corrosion behavior of niobium bearing cold deformed austenitic stainless steels in 3.5 % NaCl solution, *Materials Letters*, Vol. 6, 2007, pp. 2827–2832.

[3]. A. I. Zaky Farahata, T. El-Bitar, Eman El-Shenawy, Austenitic stainless steel bearing Nb compositional and plastic deformation effects, *Materials Science and Engineering*, Vol. 492, 2008, pp. 161–167.

[4]. C. Jullien, T. Bénézech, B. Carpentier, V. Lebret, C. Faille, Identification of surface characteristics relevant to the hygienic status of stainless steel for the food industry, *Food Engineering*, Vol. 56, 2002, pp. 77–87.

[5]. M. Finšgar, I. Milošev, Corrosion behavior of stainless steels in aqueous solutions of methanesulfonic acid, *Corrosion Science*, Vol. 52, 2010, pp. 2430–2438.

[6]. W. Kuang, E.-H. Han, X. Wu, J. Rao, Microstructural characteristics of the oxide scale formed on 304 stainless steel in oxygenated high temperature water, *Corrosion Science*, Vol. 52, 2010, pp. 3654–3660.

[7]. Z. Lu, T. Shoji, T. Dan, Y. Qiu, T. Yonezawa, The effect of roll-processing orientation on stress corrosion cracking of warm-rolled 304L stainless steel in oxygenated and deoxygenated high temperature pure water, *Corrosion Science*, Vol. 52, 2010, pp. 2547–2555.

[8]. W. Liu, R. J. Wang, J. L. Han, X. Y. Xu, Q. Li, Microstructure and mechanical performance of resistance spot welded cold-rolled high strength austenitic stainless steel, *Mater. Process. Technology*, Vol. 210, 2010, pp. 1956–1961.

[9]. Pilar De Tiedra, Óscar Martín, Manuel López, Manuel San-Juan, Use of EPR test to study the degree of sensitization in resistance spot welding joints of AISI304 austenitic stainless steel, *Corrosion Science*, Vol. 53, 2011, pp. 1563–1570.

[10]. Shishir Pandya, K. S. Ramakrishna, A. Raja Annamalai, Anish Upadhyaya, Effect of sintering temperature on the mechanical and electrochemical properties of austenitic stainless steel, *Materials Science & Engineering*, Vol. 556, 2012, pp. 271–277.

[11]. N. Parvathavarthini, S. Mulki, R. K. Dayal, I. Samajdar, K. V. Mani, Baldev Raj, Sensitization control in AISI 316L(N) austenitic stainless steel: Defining the role of the nature of grain boundary, *Corrosion Science*, Vol. 51, 2009, pp. 2144–2150.

[12]. Mathias Breimesser, Stefan Ritter, Hans-Peter Seifert, The electrochemical microcapillary technique to study intergranular stress corrosion cracking of austenitic stainless steel on the micrometer scale, *Corrosion Science*, Vol. 55, 2012, pp. 126–132.

[13]. Ching-An Huang, Yau-Zen Chang, S. C. Chen, The electrochemical behavior of austenitic stainless steel with different degrees of sensitization in the transpassive potential region in 1 M H_2SO_4containing chloride, *Corrosion Science*, Vol. 46, 2004, pp. 1501– 1513.

[14]. Maysa Terada, Mitiko Saiki, Isolda Costa, Angelo Fernando Padilha, Microstructure and intergranular corrosion of the austenitic stainless steel 1.4970, *Journal of Nuclear Materials*, Vol. 358, 2006, pp. 40–46.

[15]. Marián Vach, Terézia Kuníková, Mária Dománková, Peter Ševcc, Ľubomír Čaplovič, Peter Gogola, Jozef Janovec, Evolution of secondary phases in austenitic stainless steels during long-term exposures at 600, 650 and 800 °C, *Materials Characterization*, Vol. 59, 2008, pp. 1792-1798.

[16]. E. H. El-Shenawy, T. El-Bitar, V. Anchev, Compositional and Plastic Deformation Effects on Strength and Microstructural Changes of Austenitic Stainless Steel Bearing Nb, in *Proceedings of the 9th International Mining, Petroleum and Metallurgical Engineering Conference*, Cairo University, February 21–24, 2005, p.109 in abstracts book (full procedure on CD).

[17]. S. M. Abbasi, A Shokuhfar, Improvement of Mechanical Properties of Cr-Ni-Mo-Cu-Ti stainless Steel with Addition of Vanadium, *International Journal of Iron and Steel Research,* Vol. 14, 2007, pp. 74-78.

[18]. P. Lacombe, B. Baroux, G. Beranger. Les aciers inoxydables, *Editions of Physics*, 1990.

[19]. Ayşe Ongun Yüce, Gülfeza Kardas, Adsorption and inhibition effect of 2-thiohydantoin on mild steel corrosion in 0.1 M HCl, *Corrosion Science*, Vol. 58, 2012, pp. 86–94.

[20]. S. Zor, M. Soncu, L. C. Apan, Corrosion behavior of G-X CrNiMoNb 18-10 austenitic stainless steel in acidic solutions, *Journal of Alloys and Compounds*, Vol. 480, 2009, pp. 885–888.

[21]. E. McCaffertty, N. Heckermann, Double Layer Capacitance of Iron and Corrosion Inhibition with Polymethylene Diamines, *Electrochemical Society*, Vol. 119, Issue 2, 1972, p. 146-154.
[22]. A. S. Hamada, L. P. Karjalainen, M. C. Somani, Electrochemical corrosion behaviour of a novel submicron-grained austenitic stainless steel in an acidic NaCl solution, *Materials Science and Engineering* , Vol. 431, 2006, pp. 211–217.
[23]. Labjar Najoua, Study of l'inhibition of the corrosion of C38 steel in medium 1M HCl by compound organo- phosphatic, Phd Thesis, 2010.
[24]. I. Ahamad, R. Prasad, M.A. Quraishi, Experimental and quantum chemical characterization of the adsorption of some Schiff base compounds of phthaloyl thiocarbohydrazide on the mild steel in acid solutions, *Materials Chemistry and Physics*, Vol. 124, 2010, pp. 1155–1165.